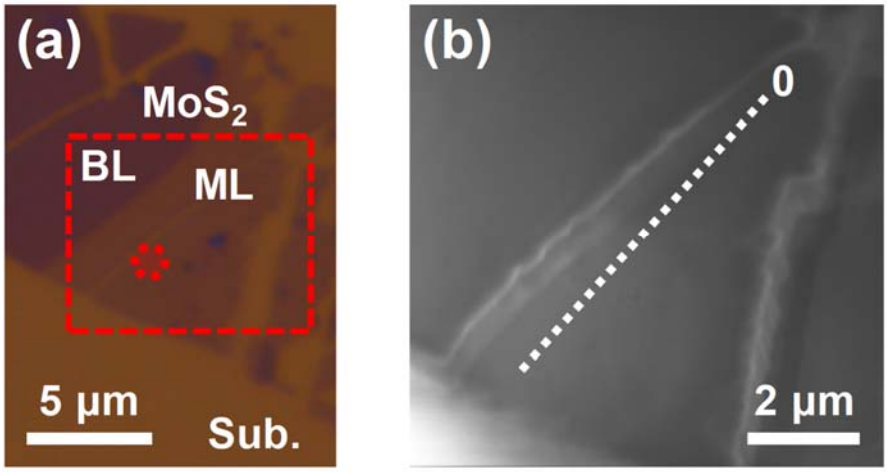

Figure S1. Scanning electron microscopy (SEM) imaging for nano-Auger electron spectroscopy (n-AES). **(a)** An optical microscopy (OM) image to show the monolayer (ML) and bilayer (BL) regions of MoS_2 flakes on SiOx/Si substrate (Sub.) with the red dashed circle indicating the spot for the selective focused-laser irradiation (FLI) process on the ML region. **(b)** A SEM image was taken from the region in the red-dashed rectangular in **(a)**. A series of spectra were obtained successively moving the focused-electron beam from the origin 0 across the irradiated region along the white dashed line with the interval of ~ 0.53 μm. It is worthy to note that the SEM image is somewhat blurry since it was not taken at the normal setting for SEM imaging but at the setting optimal for n-AES where the filament current was set as the maximum value at the given acceleration voltage and the sample was tilted by 30^0 to deliver Auger electrons to the energy analyzer properly.

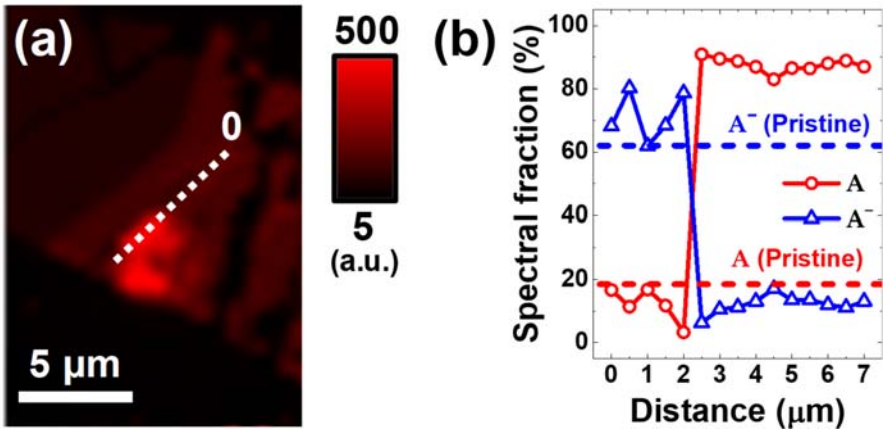

Figure S2. The spectral fractions of the ambient photoluminescence (PL) peaks contributed from the radiations of exciton (A) and negatively charged exciton (A^-), also referred to as trion. **(a)** The map of the total integrated PL intensity, I_{Total}, scanned from the ML-MoS_2 after the FLI process. (b) The spectral fractions of PL peaks of A and A^- as a function of d where d is the distance between the origin 0 and a measured

spot along the white dashed line in **(a)**. For a comparison, the average spectral fractions of the two PL peaks measured before the FLI process are included as the dashed reference lines. It can be clearly seen that the sharp transition from A^- to A occurred passing the border from the un-irradiated region ($d < 2.5$ μm) to the irradiated region ($d \geq 2.5$ μm).

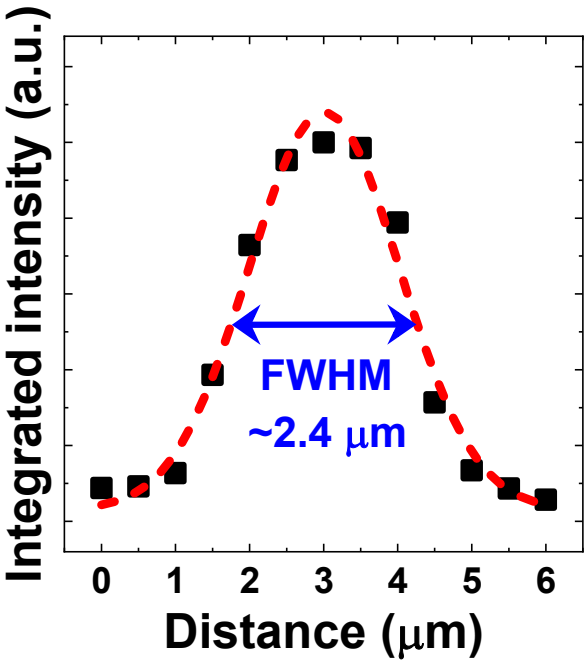

Figure S3. The Gaussian profile of the ambient PL emission profile. The profile of the sum of integrated intensities of A and A^- PL peaks, I_{A+A^-}, at room temperature in air is fitted well by the Gaussian peak. The full width at half maximum (FWHM) of the fitted peak curve (red-dashed) is given as ~2.4 μm which is very well in agreement with the laser spot size for the FLI process of ~2.3 μm. These results represent that the distribution of defects represented by the ambient PL emission would also follow the Gaussian profile of the laser beam intensity.

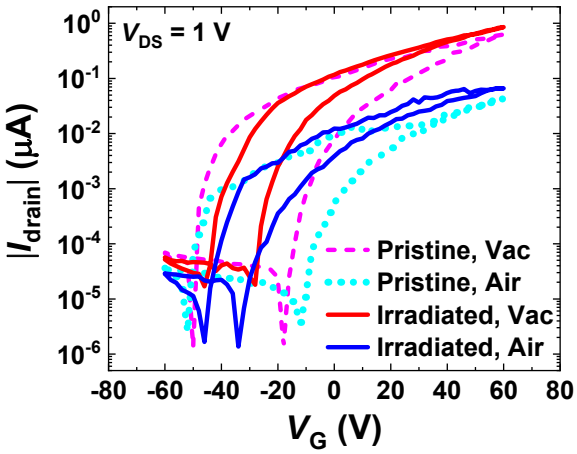

Figure S4. Vacuum annealing effects on the field-effect transistor (FET) devices based on the pristine and FLI-treated ML-MoS_2 channels. Each device was annealed in vacuum (~10^{-5} Torr) at 400 K for 4 hours and cooled down to the room temperature (RT) naturally. Then, the drain current vs. gate voltage (I_{drain} vs. V_{G}) curves were measured at the drain-to-source voltage (V_{DS}) of 1 V under the same vacuum conditions at RT. The devices were also measured in air just after the cryostat vacuum chamber was vented. For both of devices, the hysteresis could be sustained much smaller in vacuum than in air. Also, even the as-annealed devices show the much smaller hysteresis than those of un-annealed devices. The electron mobility (μ) and electron carrier concentration ($n_{2\mathrm{D}}$) of the FET channels acquired from the I_{drain} vs. V_{G} data are summarized in the Table S1.

Devices	**μ (cm^2/V·s)**	**n_{2D} (cm^{-2})**
Pristine, in vacuum	0.40	7.74×10^{12}
Pristine, in air (as-annealed)	0.50	5.37×10^{12}
Irradiated, in vacuum	0.052	3.90×10^{12}
Irradiated, in air (as-annealed)	0.031	2.88×10^{12}

Table S1. Electronic characteristics of the pristine and irradiated ML-MoS_2–based FET channels in vacuum and in air.